MDPI

Article

Confirmation of Interlayer Sulfidization of Malachite by TOF-SIMS and Principal Component Analysis

Jiushuai Deng [1,2,3,*,†] ![ID], **Hao Lai** [4,†], **Shuming Wen** [4,*] **and Shimei Li** [4]

1 School of Chemical Engineering and Energy, Zhengzhou University, Zhengzhou 450001, China
2 School of Chemical & Environmental Engineering, China University of Mining & Technology (Beijing), Beijing 100083, China
3 Department of Mechanical and Industrial Engineering, University of Toronto, Toronto M5S 3G8, Canada
4 State Key Laboratory of Complex Nonferrous Metal Resources Clean Utilization, Faculty of Land Resource Engineering, Kunming University of Science and Technology, Kunming 650093, China; kjlaihao@163.com (H.L.); shimeikm@163.com (S.L.)
* Correspondence: dengshuai689@163.com or jsdeng@mie.utoronto.ca (J.D.); shumwen@126.com (S.W.)
† The first two authors contributed equally to this paper.

✓ check for updates

Abstract: In this work, a sulfidization mechanism of malachite was confirmed based on the depth profile product, principal component, and depth profile curve analyses of time-of-flight secondary ion mass spectrometry (TOF-SIMS). The results showed that Cu/S species, including fragment ion peaks of Cu_2S^+, Cu_3S^+, S^-, HS^-, S_2^-, CuS_2^-, and CuS_3^-, were present in the inner layers of sulfidized malachite in the positive and negative spectral ranges 75–400 and 30–470 m/z. Na_2S reacted with the surface and inner atoms, causing simultaneous sulfidization of malachite on the surface and in the inner layers. The inner layer mainly contained positive fragment ions with large Cu/S ratios. In summary, the interlayer sulfidization phenomenon was confirmed and the differences in sulfidization products between the surface and inner layers were determined.

1. Introduction

Malachite is a copper-bearing carbonate mineral. It is one of the most important and common copper-bearing minerals from which copper is extracted [1–3]. For many years, flotation has been the main method for recovering malachite. In essence, the malachite is pre-sulfidized with sulfidizing agents such as sodium sulfide or sodium hydrosulfide [4]. A xanthate collector is then added for flotation [4–6]. After the addition of sodium sulfide, the surface of the oxidized mineral quickly adsorbs S^{2-} or HS^- to form a metal sulfide film [7,8]. Interactions between malachite and the collector are promoted, which improves the flotation recovery of malachite.

The process and mechanism of malachite sulfidization has been examined in previous research studies. Zhou and Chander [9] investigated the kinetics of malachite sulfidization, with sodium hydrosulfide and tetrasulfide as the sulfidizing agents. The sulfidization reaction involves the formation of a primary sulfidized layer and two secondary reactions [9]. One is the precipitation of copper ions, which diffuse through the primary layer; the other is the oxidation of the sulfidizing agent to oxysulfide species [9]. Feng et al. [10] studied the copper sulfide species formed on malachite surfaces in relation to flotation. Their results demonstrated that the flotation recovery of malachite was correlated with the contents of sulfidization products and their active components, as well as the residual sulfide ion species in pulp solutions [10]. The sulfidization product was composed of cuprous monosulfide, cuprous disulfide, and cuprous polysulfide. Among them, disulfide and polysulfide

positively contributed to the activity of the product [10]. Castro et al. [11] discussed the chemical factors in the sulfidization of copper oxide and found that besides the sulfidization with the formation of a copper sulfide layer, substantial oxidation of sulfide ions takes place at the surface of the solid. Burkitseterkyzy et al. [12] studied the material composition of raw materials and the thermodynamic analysis of ore sulfidization. It was shown that in the temperature range 298.15–500 K, the formation of copper (II) sulfide and sulfur (IV) oxide in the interaction of oxidized copper minerals with elemental nanosized sulfur is most likely [12]. Kinetic data show that the sulfidization process is controlled by a mixture of diffusion and oxidation reactions [9]. Other scholars [11,13–15] proposed some hypotheses regarding the sulfidization mechanism of malachite based on the phenomena they found.

Previous researchers considered that sulfidization reactions of malachite occurred mainly at the surface of malachite. However, in our earlier work, results of density functional theory (DFT) calculations indicated that sulfur ions could enter the interlayer of malachite, which produced the interlayer sulfidization phenomenon [16]. However, this finding needs to be further confirmed by other research methods. Time-of-flight secondary ion mass spectrometry (TOF-SIMS) is a sensitive technique for detection of all elements of the periodic table [17,18]. TOF-SIMS has a detection limit of parts per million or parts per billion for most substances [19]. The conclusions of S. Chehreh Chelgani and B. Hart [19] indicated that TOF-SIMS, as a unique surface analysis technique, can potentially provide direct determination of the parameters which control surface reactivity and, consequently, plays an important role in determining the flotation behavior of minerals [20–22]. In this work, interlayer sulfidization of malachite was confirmed on the basis of TOF-SIMS depth profile product, principal component, and depth profile curve analyses.

2. Materials and Methods

2.1. Materials

Pure malachite samples were collected from the Dongchuan copper deposit, Yunnan Province, China and subjected to manual crushing and handpicking. The isolated high-purity samples were dry ground in an agate mortar and dry-screened to obtain fractions with different particle sizes. In order to determine the purity of the sample, chemical analysis was performed on the malachite, and Table 1 shows the results. There were lower levels of impurities, such as SiO_2, MgO, CaO, Fe, and Al_2O_3. The copper grade of the sample was 56.02%, which is similar to the theoretical grade of copper in malachite (57.57%). Moreover, the malachite had a high purity of about 97%. The X-ray diffraction analysis (XRD) patterns and crystal structure of malachite are shown in Figure 1. Globally, layered malachite is widely distributed [23–25]. It is easier now to synthesize various types of mineral crystals, and to determine their properties [26–28]. Layered malachite has been artificially synthesized [15,29,30]. The malachite was sulfidized by adding analytical grade $Na_2S\cdot9H_2O$. Analytical grade NaOH was used for pH adjustment. Deionized water was used in all experiments.
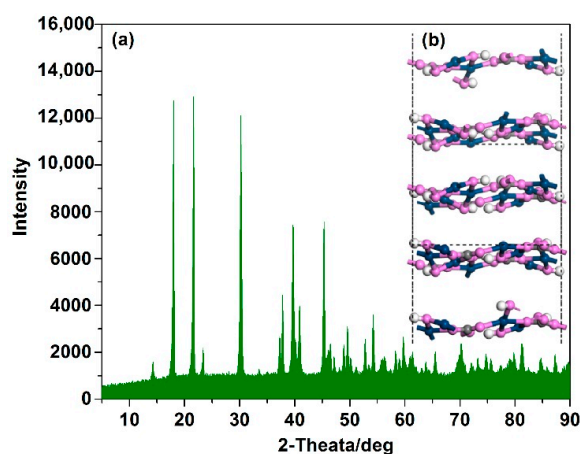
Figure 1. XRD pattern (**a**) and structural model (**b**) of malachite crystals [31,32].

Table 1. Chemical composition of the sample.

Element	Cu	Fe	SiO_2	Al_2O_3	CaO	MgO
Content (%)	56.02	0.11	0.85	0.008	0.09	0.14

2.2. Procedure of Sulfidization

The pure malachite sample was broken into pieces of approximately $1 \times 0.8 \times 0.5$ cm^3, which were polished using a polishing machine. The mineral sample was placed in a 50 mL beaker with deionized water (40 mL) and washed with an ultrasonic cleaner for 5 min. The upper cleaning fluid was removed after static clarification, and then washed three times with deionized water. The pH of the suspension was adjusted with NaOH to pH 9, and then Na_2S solution of concentration 5×10^{-4} mol/L was added to the pulp solution and absorbed for 15 min. A control experiment without Na_2S was also performed.

2.3. TOF-SIMS Analysis

A TOF-SIMS V (IONTOF GmbH, Münster, Germany) instrument was used to acquire depth profiles of the multilayer films [33,34]. TOF-SIMS depth profile analysis of malachite reacted with Na_2S for 15 min and a malachite control sample was performed at pH 9. A 15 keV Bi^{3+} source was used as the main gun and an oxygen source was used as the sputter gun. It is worth noting that, the use of a O_2 gun as an etching gun may cause lattice damage to the surface, preferential sputtering, and surface atom mixing. Therefore, a relatively low O_2 energy of 0.5 keV was used. This "knock-on" effect is weaker compared to other typical O_2 guns of 1000 and 2000 keV. An electron neutralization gun was used to neutralize any excess charge generated during sputtering. The analytical procedure was as follows. First, the main gun was used to scan a surface area of 100×100 μm^2 for 6.25 s. The main gun was then stopped and the sputter gun was loaded. The sputter gun was used to etch an area of 400×400 μm^2 at an etching rate of about 0.1964 nm/s. After etching for 2 s, sputtering was suspended. The electron neutralizing gun was then used to electronically neutralize the sputtered surface for 0.5 s. The process was repeated and the procedure was stopped after 32 scans with the main gun. The scanning time was 200 s. Data acquisition and subsequent data processing were performed using SurfaceLab (6.7, ION-TOF GmbH, Münster, Germany).

3. Results and Discussion

3.1. Determination of Sulfidization Species from TOF-SIMS Depth Profile

The aim of TOF-SIMS depth profile analyses was to determine the sulfidization products inside the malachite. Mass spectra of sulfidized and unsulfidized malachite at different depths were obtained, including cumulative mass spectra from scans 1–8, 9–16, 17–24, and 25–32. The total scanning time for each cumulative mass spectrum was 50 s. Figure 2 shows the cumulative mass spectra at different depths.

The mass spectra in Figure 2a–c show strong fragment ion peaks from Cu_2S^+, Cu_3S^+, and $Cu_5H_2S_2^+$, respectively, in the 75–400 m/z positive segment of the sulfidized malachite throughout the entire depth range. In the 30–470 m/z negative segment, fragment ion peaks from S^-, HS^-, S_2^-, CuS_2^-, $CuS_4O_2H^-$, and CuS_3^- were detected. These results show that sulfur ions reacted with the surface and inner atoms of malachite, resulting in simultaneous sulfidization of the surface and inner layers of malachite. This confirms that interlayer sulfidization occurred. Sulfidized malachite has similar positive or negative spectra at different depth ranges, which indicates that the sulfidization products of malachite are similar at different depth ranges. It was concluded that external sulfide ions synchronously enter different inner regions of malachite.
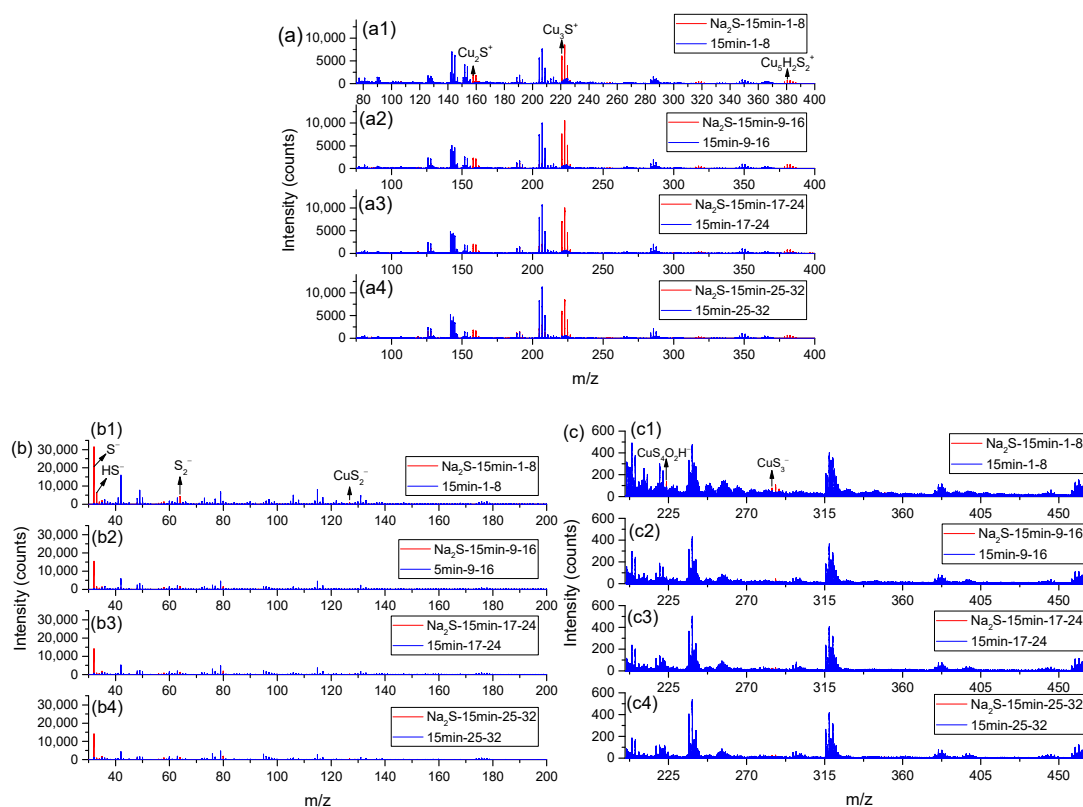
Figure 2. Cumulative mass spectra at different depths at pH 9: (**a**) positive spectrum; (a1–a4) are cumulative positive spectra obtained from scans 1–8, 9–16, 17–24, and 25–32, respectively; (**b**) and (**c**) negative spectra; (b1) (c1), (b2) (c2), (b3) (c3), and (b4) (c4) are cumulative negative spectra obtained from scans 1–8, 9–16, 17–24, and 25–32, respectively. Red and blue lines represent sulfidized and unsulfidized malachite, respectively.

3.2. Principal Component Analysis

The analytical results in Section 3.1 show that the inner layers of malachite are simultaneously sulfidized by Na$_2$S. The intensities of important fragment ion peaks by principal component analysis in multivariate statistical analysis were analyzed [34,35]. Principal component analysis is used to enrich the information obtained from multivariable systems [17]. The minimum number of newly generated variables were selected to reflect most of the information in the original variables. Among independent principal components, the first principal component has the largest variance contribution rate. The proportions of principal components in the total variance decrease in descending order. The TOF-SIMS data contain tens of thousands of fragment ion peaks, and principal component analysis is therefore an effective method for analyzing mass spectroscopic data [36,37].

In the present study, 32 independent mass spectra—in depth order from the total mass spectrum obtained from 32 scans—were read. The scan analysis time for each mass spectrum was 6.25 s, with a depth interval of about 0.3928 nm between the mass acquisition surfaces. For the first and 32nd mass spectra, the acquisition depths were 0 and 12.1768 nm. After uniform mass calibration of the mass spectra, the important fragment ion peaks were selected for principal component analysis. The raw data were usually preprocessed before principal component analysis. We divided the intensity of each selected fragment ion peak by the total intensity of fragment ion peaks for normalization and standardization. The intensity variance of a treated fragment ion peak is equal to 1. Figure 3 shows the principal component analysis results for the positive spectra of sulfidized malachite at 32 different depths. PC1 and PC2 respectively represent the loadings or scores in the transverse and longitudinal directions in Figure 3.
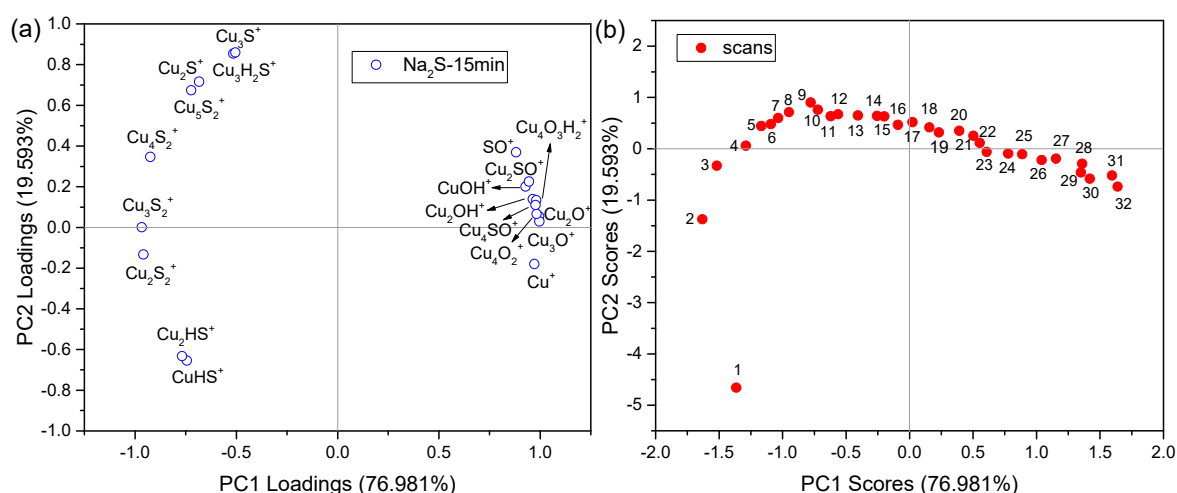
Figure 3. The principal component analysis results for positive spectra of sulfidized malachite at 32 different depths. (**a**): Loadings plot of PCs 1 and 2; (**b**): Scores plot of PCs 1 and 2.

The copper–sulfur-containing and copper–oxygen-containing positive fragment ions have negative and positive loadings, respectively, in PC1, which is consistent with the fact that the sulfidized malachite consists of copper–sulfur-containing compounds. PC1 therefore represents the sulfidization degree of malachite. The sulfur-containing positive fragment ions have different loadings in PC2, indicating that these sulfur-containing fragment ions originate from different compounds. PC2 therefore represents the difference of sulfidization products.

Figure 3b shows that the 32 positive spectra are well separated in a score plot. The scores for scans 1–32 in PC1 gradually increase from negative to positive. Figure 4a indicates that the sulfidization degree of malachite decreases with increasing etching depth. This is in line with the characteristics of the sulfidization process in that sulfur-containing components can easily diffuse from the solution to the surface and interlayers of malachite. However, it become difficult for the sulfur-containing components to diffuse deeper into the interlayers. A smaller distance from the surface or cross section leads to a higher sulfidization degree of malachite. This is consistent with the findings of Castro et al. [11,38].
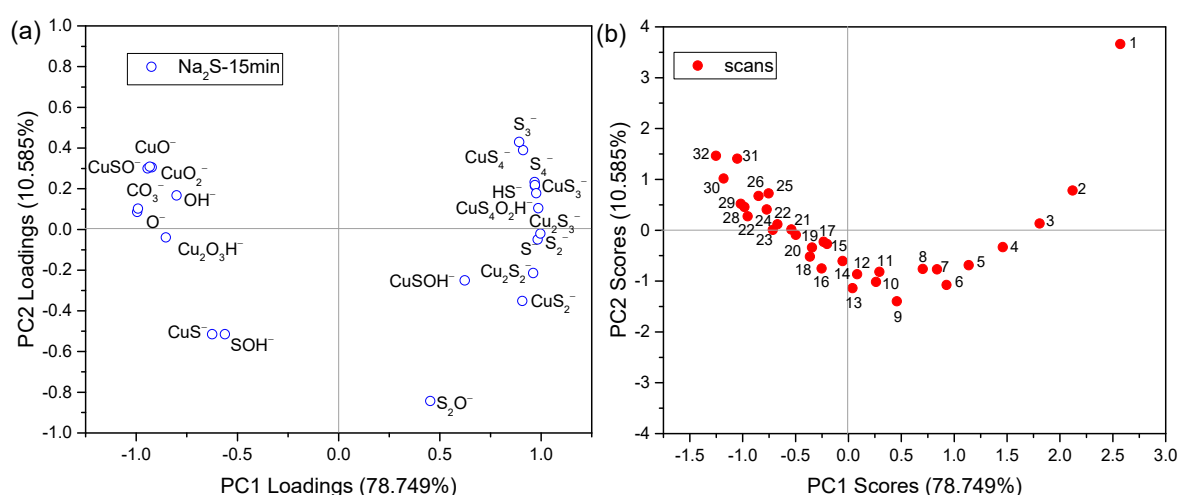
Figure 4. Principal component analysis results for TOF-SIMS negative spectra of sulfidized malachite at 32 different depths. (**a**): Loadings plot of PCs 1 and 2; (**b**): Scores plot of PCs 1 and 2.

The scores for scans 1–32 in PC2 gradually change from negative to positive, and then to negative again. This indicates that different sulfides are formed at different depths during interlayer

sulfidization. The first scan (depth = 0 nm) had the smallest negative score and the largest distance from other points in PC2. Hence, there is a significant difference in the sulfur-containing compounds between the surface and inner layers. The results also show that scans 1–3 had strong correlations with $CuHS^+$, Cu_2HS^+, and $Cu_2S_2^+$, while scans 4–22 were strongly correlated with $Cu_3S_2^+$, $Cu_4S_2^+$, $Cu_5S_2^+$, Cu_2S^+, Cu_3S^+, $Cu_3H_2S^+$, Cu_4SO^+, Cu_2SO^+, and SO^+. The copper–oxygen-containing substance had a small positive score in PC2, while scans 23–32 had negative scores in PC2. This shows that scans 23–32 have strong negative correlations with positive fragment ions such as $Cu_3S_2^+$, $Cu_4S_2^+$, $Cu_5S_2^+$, Cu_2S^+, Cu_3S^+, and $Cu_3H_2S^+$.

Figure 4 shows the principal component analysis results of the negative fragment ions. The results show that the negative fragment ions were more discrete than the positive fragment ions in the load plot. On the basis of the degree of dispersion, most of the negative fragment ions can be divided into two types. The first is negative fragment ions produced from sulfidization products: S_3^-, CuS_4^-, S_4^-, HS^-, CuS_3^-, $CuS_4O_2H^-$, $Cu_2S_3^-$, S^-, S_2^-, $Cu_2S_2^-$, CuS_2^-, and $CuSOH^-$; the second includes negative fragment ions from basic copper carbonate: $Cu_2O_3H^-$, O^-, CO_3^-, OH^-, CuO_2^-, $CuSO^-$, and CuO^-. The first and second types of negative fragment ions have positive and negative loadings, respectively, in PC1. Therefore, PC1 represents the sulfidization degree of malachite. However, there are significant differences between the loadings of sulfur-containing negative fragment ions in PC2, indicating that these fragments originate from different compounds. Therefore, PC2 represents the difference between the sulfidization products.

Figure 4b shows that the 32 negative spectra are well separated in the score plot. From scan 1 to scan 32, the PC1 score gradually decreased from positive to negative. The combined results in Figure 4a,b led to the conclusion that the sulfidization degree of malachite decreased with increasing etching depth. Similarly, the scores for scan 1 to scan 32 for PC2 gradually change from positive to negative, and then to positive. This indicates that sulfidized malachite contains different sulfidization species at different depths. The first scan (depth = 0 nm) had the largest positive score and the largest distance from other points in PC2. Therefore, there is a significant difference of sulfur-containing compounds between the surface and inner of sulfidized malachite. According to the results in Figure 4a, we can see that scans 1–3 had strong correlations with S_3^-, CuS_4^-, S_4^-, HS^-, CuS_3^-, $CuS_4O_2H^-$, $Cu_2S_3^-$, S^-, and S_2^-; scans 4–21 were strongly correlated with $Cu_2S_2^-$, CuS_2^-, $CuSOH^-$, S_2O^-, CuS^-, and SOH^-, and scans 22–32 had strong negative correlations with negative fragment ions such as $Cu_2O_3H^-$, O^-, CO_3^-, OH^-, CuO_2^-, $CuSO^-$, and CuO^-.

Combining the results of principal component analysis of positive and negative ion fragments, we also found that fragment ions with small Cu/S ratios dominate in the superficial layer of malachite (i.e., scans 1–3, depth: 0–0.7856 nm). In the middle layer, i.e., scans 4–21 (depth: 1.1784–7.856 nm), the fragment ions with large Cu/S ratios and those containing sulfur and oxygen affect the results more, with the greatest effect observed for scan 9 (depth = 3.1424 nm). In the deep layer, i.e., scans 22–32 (depth: 8.2488–12.1768 nm), mass spectrometry information was mainly affected by fragment ions produced by malachite itself, with a low sulfidization degree.

3.3. Depth Profile Curve Analysis

As discussed in Section 3.2, principal component analysis shows that the sulfidized malachite had different sulfidization compositions at different depths, therefore, the variations of various fragment ions with depth using depth profile curve analysis of TOF-SIMS was investigated.

The depth profile curves of the positive fragment ions in Figure 5a,b show that the curves can be broadly divided into three categories. The blue line represents the first type: $CuHS^+$, Cu_2HS^+, and $Cu_2S_2^+$, whose fragment ion intensity decreased with increasing etching depth. The red line represents the second type: $Cu_3S_2^+$, $Cu_4S_2^+$, $Cu_5S_2^+$, Cu_2S^+, Cu_3S^+, and $Cu_3H_2S^+$, whose fragment ion intensity first increased and then decreased with increasing etching depth. The orange line represents the third type: Cu^+, Cu_3O^+, Cu_2O^+, $Cu_4O_2^+$, Cu_4SO^+, $CuOH^+$, Cu_2SO^+, $Cu_4O_3H_2^+$, Cu_2OH^+, and SO^+, whose fragment ion intensity increased with increasing etching depth.
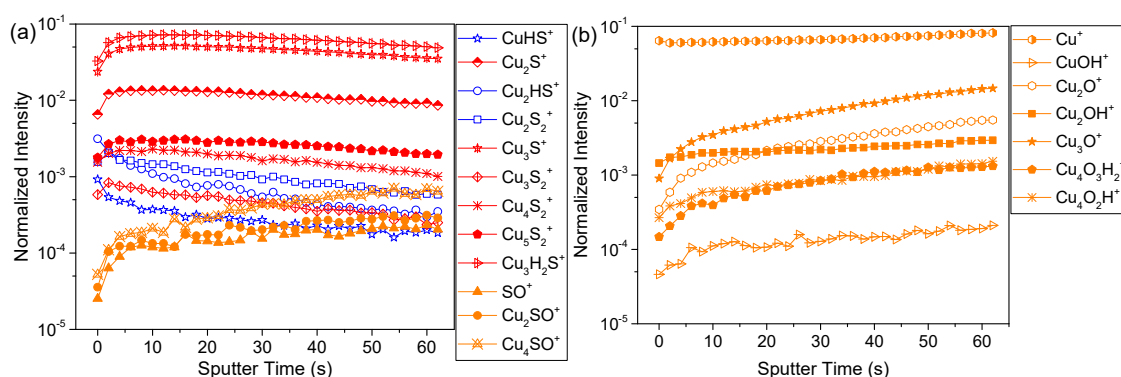
Figure 5. The depth profile curves for positive ions of sulfidized malachite: (**a**) sulfur containing positive fragment ions and (**b**) oxygen-containing positive ion and Cu^+ fragments.

The above analysis suggests that the sulfidization mechanism at the surface is different from that in the inner layers. The malachite discussed in this study had a layered structure. The minimum distance between copper atoms in adjacent layers of malachite is 0.393 nm, which is larger than the diameter of S^{2-}, i.e., 0.368 nm; S^{2-} can therefore theoretically enter the interlayers of malachite [16]. The characteristics of fragment ions such as $Cu_3S_2^+$, $Cu_4S_2^+$, $Cu_5S_2^+$, Cu_2S^+, Cu_3S^+, and $Cu_3H_2S^+$ indicate that S^{2-} or HS^- is probably connected to the copper atoms in the upper and lower layers, to form Cu_{top}–S_{middle}–Cu_{bottom}.

At the malachite surface, the sulfur components in the solution react with the copper atoms in the same layer to generate copper–sulfur-containing compounds. These substances produce positive fragment ions with small Cu/S ratios—$CuHS^+$ and Cu_2HS^+—which is defined as surface sulfidization. The sulfur-containing component that diffuses from the surface to the interlayer simultaneously reacts with copper atoms in upper and lower layers to form another copper–sulfur-containing compound, which is defined as the transition layer sulfidization. The sulfur component intercalates into the interlayer from the cross section of the lamellar structure, which can be defined as the interlayer sulfidization mode. The transition layer and interlayer sulfidization give positive fragment ions with large Cu/S ratios: $Cu_3S_2^+$, $Cu_4S_2^+$, $Cu_5S_2^+$, Cu_2S^+, Cu_3S^+, and $Cu_3H_2S^+$. Steric hindrance exists during the diffusion of sulfur-containing components from the surface and cross sections to the interior of malachite. The intensity of the second type of positive fragment ion therefore decreases after initially increasing. Due to a decrease in the number of copper-containing sites and the increased steric hindrance, sulfidization of the same layer weakens with increasing depth, and the intensity of the first type of positive fragment ion therefore decreases with increasing depth.

The depth profile curves of negative fragment ions in Figure 6 show that the intensities of different negative fragment ions vary with changes in depth. This is in accordance with the fact that negative fragment ions are more discrete in Figure 5a, which is similar to the results of the analysis of positive ion depth profiles. The species represented by red lines, i.e., the negative fragment ions, including S_3^-, CuS_4^-, S_4^-, HS^-, CuS_3^-, $CuS_4O_2H^-$, $Cu_2S_3^-$, and S_2^-, are mainly derived from surface sulfidization products. The species represented by blue and pink lines, i.e., S^-, CuS_2^-, $Cu_2S_2^-$, $CuSOH^-$, CuS^-, and SOH^-, possibly originate from both the same layer and interlayer sulfidization products, while S_2O^- mainly comes from interlayer sulfidization products.

For Cu_4SO^+, Cu_2SO^+, and SO^+ in Figure 4a, and $CuSO^-$ in Figure 5a, the intensities increase with increasing depth. This type of fragment ion may represent another interlayer sulfidization mode, namely, Cu_{top}–S_{middle}–O_{bottom} sulfidization. This mode may be more incidental than Cu_{top}–S_{middle}–Cu_{bottom} sulfidization. Therefore, the intensities of these fragment ions increase with increasing etching depth. However, it cannot be ignored that O_2 was used as the etching gas in this study [39,40]. As the etching depth increases, the amount of oxygen-containing fragment ions from malachite increases. Consequently, oxygen-containing, sulfur-containing, and copper-containing fragment ions may recombine to form new Cu–S–O fragment ions.
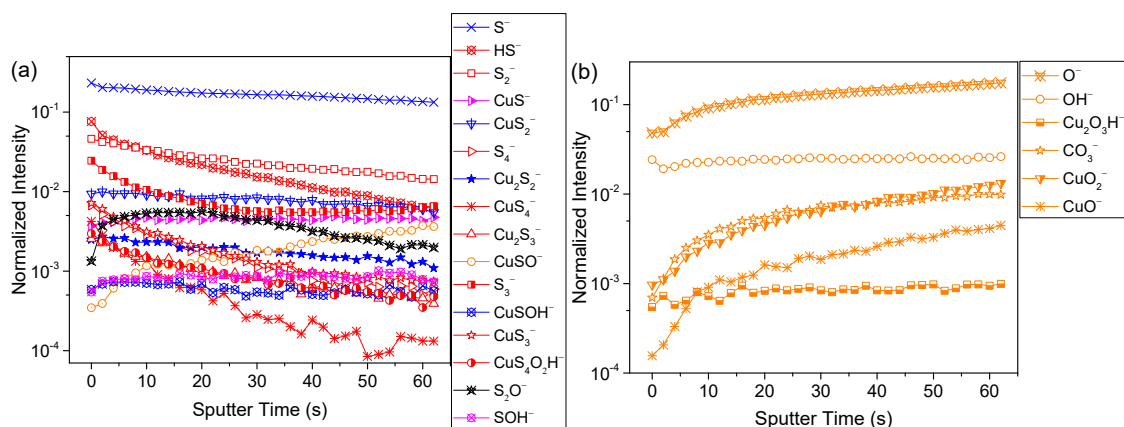
Figure 6. Depth profile curves for negative ions of sulfidized malachite: (**a**) sulfur-containing negative fragment ions and (**b**) oxygen-containing negative ions and Cu^+ fragments.

4. Conclusions

In this study, TOF-SIMS depth profile product analysis, principal component analysis, and depth profile curve analysis were used to confirm a novel interlayer sulfidization of malachite. The conclusions are as follows.

(1) The depth profile product analysis showed that there were strong fragment ion peaks from Cu_2S^+, Cu_3S^+, and $Cu_5H_2S_2^+$ in the 75–400 m/z positive segment of the sulfidized malachite spectrum throughout the entire depth range. In the 30–470 m/z negative segment, fragment ion peaks, including S^-, HS^-, S_2^-, CuS_2^-, $CuS_4O_2H^-$, and CuS_3^-, were detected. These results showed that sulfur ions reacted with the surface and inner atoms of malachite, resulting in simultaneous sulfidization at the surface and inner layers.

(2) Principal component analysis showed that the sulfidized malachite products consisted of copper–sulfur-containing compounds, while the unsulfidized malachite consisted of copper–oxygen-containing compounds. There were significant differences in the sulfidization compounds between the surface and inter layers of malachite.

(3) The depth profile curve analysis showed that there were different sulfide compositions at different depths. Fragment ions with small Cu/S ratios dominated in the superficial layer, while fragment ions with large Cu/S ratios and those containing sulfur and oxygen were more prominent in the inner layers.

In summary, in this study, the interlayer sulfidization phenomenon was confirmed and the differences in sulfidization products between the surface and inner layers were determined.

References

1.　Xian, Y.J.; Wang, Y.J.; Wen, S.M.; Nie, Q.; Deng, J.S. Floatability and oxidation of pyrite with different spatial symmetry. *Miner. Eng.* **2015**, *72*, 94–100. [CrossRef]

2.　Lee, K.; Archibald, D.; McLean, J.; Reuter, M. Flotation of mixed copper oxide and sulphide minerals with xanthate and hydroxamate collectors. *Miner. Eng.* **2009**, *22*, 395–401. [CrossRef]

3.　Wu, D.; Ma, W.; Mao, Y.; Deng, J.; Wen, S. Enhanced sulfidation xanthate flotation of malachite using ammonium ions as activator. *Sci. Rep.* **2017**, *7*, 2086. [CrossRef] [PubMed]

4.　Kanda, J.-M.; Kongolo, M.; Gaydardzhiev, S.; De Donato, P.; Barres, O.; Bastin, D. Insights upon the adsorption mechanism of KAX on malachite. In Proceedings of the XXVII International Mineral Processing Congress, Santiago, Chile, 20–24 October 2014.

5.　Gao, Q.; Su, J.; Qin, G. Several Problem of Oxide Copper Sulphidizing Flotation. *Non-Ferous Min. Metall.* **2003**, *19*, 22–23. (In Chinese)

6.　Soto, H.; Laskowski, J. Redox conditions in the flotation of malachite with sulphidizing agent. *Trans. Inst. Min. Met. C Min. Process. Extr. Met.* **1973**, *82*, C153–C157.

7.　Fang, J.; Li, Y. Study on technological mineralogy and concentration of oxide copper ore. *Yunnan Metall.* **2005**, *34*, 50–53. (In Chinese)

8.　Qiu, T.; Ding, S.; Zhang, B.; Yan, S. Application situation of sodium sulfide in the flotation. *Nonferrous Met. Sci. Eng.* **2013**, *3*, 39–43. (In Chinese)

9.　Zhou, R.; Chander, S. Kinetics of sulfidization of malachite in hydrosulfide and tetrasulfide solutions. *Int. J. Miner. Process.* **1993**, *37*, 257–272. [CrossRef]

10.　Feng, Q.; Zhao, W.; Wen, S.; Cao, Q. Copper sulfide species formed on malachite surfaces in relation to flotation. *J. Ind. Eng. Chem.* **2017**, *48*, 125–132. [CrossRef]

11.　Castro, S.; Goldfarb, J.; Laskowski, J. Sulphidizing reactions in the flotation of oxidized copper minerals, I. Chemical factors in the sulphidization of copper oxide. *Int. J. Miner. Process.* **1974**, *1*, 141–149. [CrossRef]

12.　Burkitseterkyzy, G.; Katkeeva, G.L.; Oskembekov, I.M.; Gizatullina, D.R.; Zhunussov, A.M. Study of the Material Composition of Raw Materials and the Thermodynamic Analysis of Ore Sulphidization. 2017. Available online: http://chemistry-vestnik.ksu.kz/apart/2017-88-4/8.pdf (accessed on 2 February 2019).

13.　Gaudin, A.M. *Flotation*; McGraw-Hill: New York, NY, USA, 1957.

14.　Liu, D.; Zhang, W.; Wen, S. *Flotation Technology of Copper Oxide Ore*; Metallurgical Industry Press: Beijing, China, 2009. (In Chinese)

15.　Park, K.; Park, S.; Choi, J.; Kim, G.; Tong, M.; Kim, H. Influence of excess sulfide ions on the malachite-bubble interaction in the presence of thiol-collector. *Sep. Purif. Technol.* **2016**, *168*, 1–7. [CrossRef]

16.　Wu, D.; Mao, Y.; Deng, J.; Wen, S. Activation mechanism of ammonium ions on sulfidation of malachite (–201) surface by DFT study. *Appl. Surf. Sci.* **2017**, *410*, 126–133. [CrossRef]

17.　Pacholski, M.L. Principal component analysis of TOF-SIMS spectra, images and depth profiles: An industrial perspective. *Appl. Surf. Sci.* **2004**, *231*, 235–239. [CrossRef]

18.　Bertrand, P.; Lu-Tao, W. Time-of-flight secondary ion mass spectrometry (ToF-SIMS). In *Microbeam and Nanobeam Analysis*; Springer: New York, NY, USA, 1996; pp. 167–182.

19.　Chelgani, S.C.; Hart, B. TOF-SIMS studies of surface chemistry of minerals subjected to flotation separation—A review. *Miner. Eng.* **2014**, *57*, 1–11. [CrossRef]

20.　Liu, J.; Wang, Y.; Luo, D.; Chen, L.; Deng, J. Comparative study on the copper activation and xanthate adsorption on sphalerite and marmatite surfaces. *Appl. Surf. Sci.* **2018**, *439*, 263–271. [CrossRef]

21.　Boulton, A.; Fornasiero, D.; Ralston, J. Characterisation of sphalerite and pyrite flotation samples by XPS and ToF-SIMS. *Int. J. Miner. Process.* **2003**, *70*, 205–219. [CrossRef]

22.　Priest, C.; Stevens, N.; Sedev, R.; Skinner, W.; Ralston, J. Inferring wettability of heterogeneous surfaces by ToF-SIMS. *J. Colloid Interface Sci.* **2008**, *320*, 563–568. [CrossRef] [PubMed]

23.　Wells, A. Malachite: Re-examination of crystal structure. *Acta Crystallogr.* **1951**, *4*, 200–204. [CrossRef]

24.　Süsse, P. Verfeinerung der kristallstruktur des malachits, $Cu_2(OH)_2CO_3$. *Acta Crystallogr.* **1967**, *22*, 146–151. [CrossRef]

25.　Zigan, F.; Joswig, W.; Schuster, H.; Mason, S. Verfeinerung der Struktur von Malachit, $Cu_2(OH)_2CO_3$, durch Neutronenbeugung. *Z. Für Krist.-Cryst. Mater.* **1977**, *145*, 412–426. [CrossRef]

26. Deng, J.; Li, S.; Zhou, Y.; Liang, L.; Zhao, B.; Zhang, X.; Zhang, R. Enhancing the microwave absorption properties of amorphous CoO nanosheet-coated Co (hexagonal and cubic phases) through interfacial polarizations. *J. Colloid Interface Sci.* **2018**, *509*, 406–413. [CrossRef] [PubMed]

27. Deng, J.; Wang, Q.; Zhou, Y.; Zhao, B.; Zhang, R. Facile design of a ZnO nanorod–Ni core–shell composite with dual peaks to tune its microwave absorption properties. *RSC Adv.* **2017**, *7*, 9294–9302. [CrossRef]

28. Zhao, B.; Guo, X.; Zhao, W.; Deng, J.; Shao, G.; Fan, B.; Bai, Z.; Zhang, R. Yolk–Shell Ni@ SnO_2 Composites with a Designable Interspace To Improve the Electromagnetic Wave Absorption Properties. *ACS Appl. Mater. Interfaces* **2016**, *8*, 28917–28925. [CrossRef]

29. Choi, J.; Choi, S.Q.; Park, K.; Han, Y.; Kim, H. Flotation behaviour of malachite in mono-and di-valent salt solutions using sodium oleate as a collector. *Int. J. Miner. Process.* **2016**, *146*, 38–45. [CrossRef]

30. Tanaka, H.; Yamane, M. Preparation and thermal analysis of synthetic malachite $CuCO_3 \cdot Cu(OH)_2$. *J. Therm. Anal. Calorim.* **1992**, *38*, 627–633. [CrossRef]

31. Natarajan, S.; Mandal, S. Open-Framework Structures of Transition-Metal Compounds. *Angew. Chem. Int. Ed.* **2008**, *47*, 4798–4828. [CrossRef]

32. Feng, P.; Bu, X.; Zheng, N. The interface chemistry between chalcogenide clusters and open framework chalcogenides. *Acc. Chem. Res.* **2005**, *38*, 293–303. [CrossRef] [PubMed]

33. Rinnen, S.; Stroth, C.; Riße, A.; Ostertag-Henning, C.; Arlinghaus, H.F. Characterization and identification of minerals in rocks by ToF-SIMS and principal component analysis. *Appl. Surf. Sci.* **2015**, *349*, 622–628. [CrossRef]

34. Smart, R.S.C.; Gerson, A.R.; Biesinger, M.C.; Hart, B.R. The development of statistical TOF-SIMS applied to minerals recovery by froth flotation. *Surf. Interface Anal.* **2017**, *49*, 1387–1396. [CrossRef]

35. Holzweber, M.; Heinrich, T.; Kunz, V.; Richter, S.; Traulsen, C.H.-H.; Schalley, C.A.; Unger, W.E. Principal component analysis (PCA)-assisted time-of-flight secondary-ion mass spectrometry (ToF-SIMS): A versatile method for the investigation of self-assembled monolayers and multilayers as precursors for the bottom-up approach of nanoscaled devices. *Anal. Chem.* **2014**, *86*, 5740–5748. [CrossRef]

36. Pachuta, S.J. Enhancing and automating TOF-SIMS data interpretation using principal component analysis. *Appl. Surf. Sci.* **2004**, *231*, 217–223. [CrossRef]

37. Welch, N.G.; Madiona, R.M.; Scoble, J.A.; Muir, B.W.; Pigram, P.J. ToF-SIMS and Principal Component Analysis Investigation of Denatured, Surface-Adsorbed Antibodies. *Langmuir* **2016**, *32*, 10824–10834. [CrossRef] [PubMed]

38. Castro, S.; Soto, H.; Goldfarb, J.; Laskowski, J. Sulphidizing reactions in the flotation of oxidized copper minerals, II. Role of the adsorption and oxidation of sodium sulphide in the flotation of chrysocolla and malachite. *Int. J. Miner. Process.* **1974**, *1*, 151–161. [CrossRef]

39. Chu, Y.-H.; Liao, H.-Y.; Lin, K.-Y.; Chang, H.-Y.; Kao, W.-L.; Kuo, D.-Y.; You, Y.-W.; Chu, K.-J.; Wu, C.-Y.; Shyue, J.-J. Improvement of the gas cluster ion beam-(GCIB)-based molecular secondary ion mass spectroscopy (SIMS) depth profile with O_2^+ cosputtering. *Analyst* **2016**, *141*, 2523–2533. [CrossRef]

40. Holzer, S.; Krivec, S.; Kayser, S.; Zakel, J.; Hutter, H. Large O_2 Cluster Ions as Sputter Beam for ToF-SIMS Depth Profiling of Alkali Metals in Thin SiO_2 Films. *Anal. Chem.* **2017**, *89*, 2377–2382. [CrossRef] [PubMed]